Cell Reports
Medicine

Article

Anti-IL-15 treatment reduces acute lentivirus inflammation and signaling in the brain

Graphical abstract

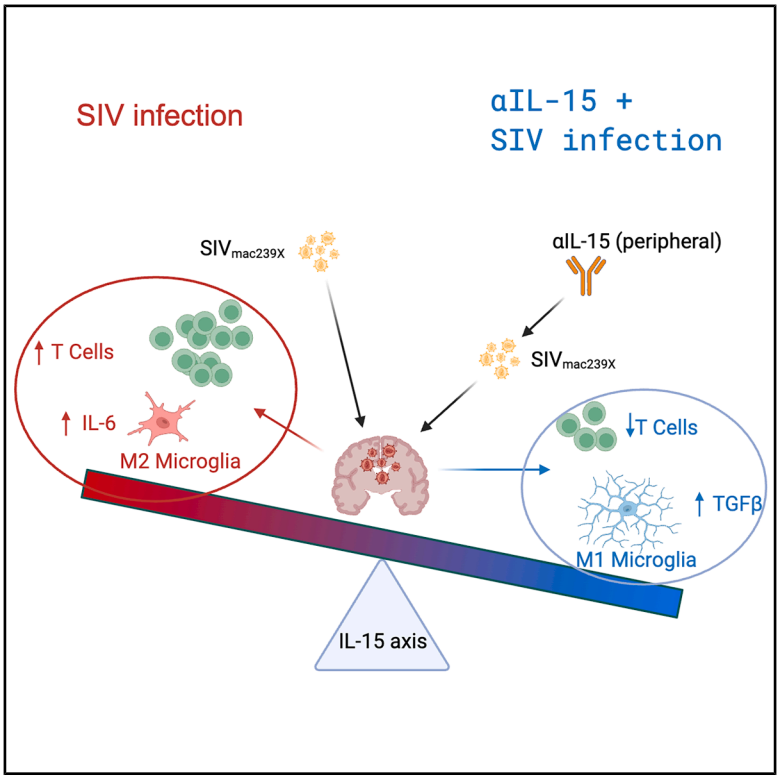

Authors

Daniel R. Ram,
Raja Mohan Gopalakrishnan,
Malika Aid, ..., Brandon F. Keele,
R. Keith Reeves, C. Sabrina Tan

Correspondence

sabrina-tan@uiowa.edu

In brief

Ram and Gopalakrishnan et al. demonstrate that peripheral cytokine modulation alters the brain's inflammatory environment and immune response to retroviral infection. These results demonstrate that a favorable central nervous system environment can be induced by intravenous administrations of antibodies. This work will inform and guide therapeutic strategies for HIV-associated neurocognitive disorder.

Highlights

- Peripheral pre-administration of αIL-15 alters CNS immune responses to acute SIV infection
- T cell quantities in the brain are reduced following peripheral αIL-15
- Pre-treatment with αIL-15 prior to SIV infection does not alter brain viral load
- Blood IL-15 quantities and elevated T cells are linked to M2 microglia phenotype in brain

Ram et al., 2026, Cell Reports Medicine 7, 102567
January 20, 2026
https://doi.org/10.1016/j.xcrm.2025.102567

CellPress

Cell Reports Medicine

CellPress
OPEN ACCESS

Article

Anti-IL-15 treatment reduces acute lentivirus inflammation and signaling in the brain

Daniel R. Ram,[1,2,12] Raja Mohan Gopalakrishnan,[1,12] Malika Aid,[1] Kyle Kroll,[3] Jasmine Miftahof,[4] Omar Aristizabal,[4] Eunice Kayitare Gikundiro,[1,4] Caitlin Davis,[1] Marco M. Hefti,[5] Kimberly L. Fiock,[5] Brook Tilahun,[1,6] Yvette Umutoniwase,[1,6] Kate Loidolt,[1,6] Christine M. Fennessey,[9] Noe B. Mercado,[1] Victoria Harper-Alexander,[2] Rhianna Jones,[3] Griffin Woolley,[3] Valerie Varner,[1] Michelle Lifton,[1] Steven E. Bosinger,[7,8] Dan H. Barouch,[1] Brandon F. Keele,[9] R. Keith Reeves,[1,3,10] and C. Sabrina Tan[1,4,11,13,*]

[1]Center for Virology and Vaccine Research, Department of Medicine, Beth Israel Deaconess Medical Center, Harvard Medical School, Boston, MA, USA
[2]Burnett School of Biomedical Sciences, College of Medicine, University of Central Florida, Orlando, FL, USA
[3]Division of Innate and Comparative Immunology, Center for Human Systems Immunology, Duke University School of Medicine, Durham, NC, USA
[4]Department of Medicine, Carver College of Medicine, University of Iowa, Iowa City, IA, USA
[5]Department of Pathology, Carver College of Medicine, University of Iowa, Iowa City, IA, USA
[6]Biology Department, Concordia College, Moorhead, MN, USA
[7]Emory Vaccine Center and Yerkes National Primate Research Center, Emory University, Atlanta, GA, USA
[8]Department of Pathology and Laboratory Medicine, Emory University School of Medicine, Atlanta, GA, USA
[9]AIDS and Cancer Virus Program, Frederick National Laboratory for Cancer Research, Frederick, MD, USA
[10]Division of Surgical Sciences, Department of Surgery, Duke University School of Medicine, Durham, NC, USA
[11]Division of Infectious Diseases, Department of Medicine, Beth Israel Deaconess Medical Center, Harvard Medical School, Boston, MA, USA
[12]These authors contributed equally
[13]Lead contact
*Correspondence: sabrina-tan@uiowa.edu
https://doi.org/10.1016/j.xcrm.2025.102567

SUMMARY

HIV-associated neurocognitive disorder (HAND) remains a significant complication in people living with HIV, with inflammation playing a central role in its pathogenesis. Understanding how the brain's immune network responds to lentiviral infection is therefore critical. We show that acute simian immunodeficiency virus (SIV) infection elicits a robust resident brain immune response in control animals, marked by enhanced microglial ramification. In contrast, animals pretreated with anti-interleukin (IL)-15 antibodies (αIL-15) before $SIV_{mac239X}$ infection display reduced neuroinflammation without altering brain viral burden. Peripheral IL-15 blockade decreases brain-infiltrating T lymphocytes, alters their spatial dynamics, suppresses proinflammatory cytokine (IL-6) expression in microglia, and increases anti-inflammatory cytokine (TGF-β) expression in brain macrophages. Transcriptomic profiling reveals a global reduction in inflammatory signaling and an upregulation of genes associated with M1 macrophage pathways. Together, these findings demonstrate that peripheral IL-15 modulation attenuates neuroinflammation during acute lentiviral infection and highlight IL-15 as a potential therapeutic target for neuroinflammatory conditions of the brain.

INTRODUCTION

Despite advancements in viral suppression with antiretroviral therapies, HIV-associated neurocognitive disorder (HAND) remains an ongoing chronic health problem in approximately half of people living with HIV (PLWH) worldwide.[1,2] HIV infects the brain within days during the acute phase of infection and causes neurological symptoms.[3] Viral entry into the central nervous system (CNS) elicits an early immune response, driving neuroinflammation and eventually leading to the development of HAND.[4] Understanding the mechanisms of neuroinflammation and identifying the contributing factors during acute infection is needed to prevent HAND. Studying simian immunodeficiency virus (SIV) infection in a rhesus macaque (RM) model, we have previously demonstrated that an elevated inflammatory immune response occurs during acute SIV infection in the brain, mirroring findings in human cerebrospinal fluid (CSF).[5] In addition, we found that inflammatory responses even precede reliable virus detection in the brain, suggesting an impact of the peripheral immune response on the CNS. Thus, we sought to elucidate the connection between the peripheral immune response and CNS neuroinflammation during acute lentiviral infection.

Interleukin-15 (IL-15) is a versatile cytokine produced by myeloid lineage cells that mediates both inflammatory and

Table 1. SIV viral load in rhesus macaque plasma and frontal cortex, thalamus, and basal ganglia at 7 and 14 days post-infection with $SIV_{mac}239X$ in both untreated and αIL-15-treated RM

Animal ID	Brain region	SIV Gag DNA copies/1e^6 cells	SIV Gag RNA copies/μg total RNA	Corresponding peripheral viral load (log_{10} copies/mL of plasma)
7 dpi (untreated)				
Rh4	FC	228	below LOD	4.31
Rh5	FC	below LOD	below LOD	4.55
Rh6	FC	below LOD	below LOD	6.12
14 dpi (untreated)				
Rh7	FC	467	4258	7.76
Rh8	FC	136	1091	4.38
Rh9	FC	377	686	8.11
Rh10	FC	68	94	7.31
Rh11	FC	143	342	6.57
Rh11	BG	37	571	see above
Rh11	TH	24	530	see above
7 dpi (αIL-15 treated)				
Rh18	FC	below LOD	below LOD	4.16
Rh19	FC	below LOD	below LOD	4.97
14 dpi (αIL-15 treated)				
Rh20	FC	126/112	1444	8.13
Rh21	FC	1413	296	7.68
Rh22	FC	653	1189	7.97
Rh23	FC	89	337	7.82
Rh23	TH	39	896	See above
Rh23	BG	99	204	See above
Rh24	FC	167	2125	8.39
Rh24	TH	220	1563	See above
Rh24	BG	179	17407	See above

Viral load was assessed through quantification of SIV Gag DNA or SIV Gag RNA. Undetectable viral DNA or RNA is represented as below the limit of detection (LOD). The untreated viral load data were already published,[5] but we are including them here to facilitate easier comparison with the αIL-15-treated group. FC, frontal cortex; TH, thalamus; BG, basal ganglia.

protective immune reactions against viral, bacterial, and parasitic pathogens by serving as a mediator between the innate and adaptive immune systems. IL-15 plays an important role, specifically in HIV and SIV infections, by contributing to the proliferation and activation of natural killer (NK) cells and antigen-specific cytotoxic T cells[6–9] to control viremia.[10] IL-15 is also important in diseases of the CNS, where increases in serum and CSF IL-15 have been observed in patients with active multiple sclerosis.[11] IL-15's role in neuroinflammation is particularly relevant to understanding the pathogenesis of HAND and other CNS disorders associated with viral infections. Peripheral IL-15 administration in experimental autoimmune encephalomyelitis (EAE) mice resulted in prolonged increases in the number of pro-inflammatory infiltrating T cells in the brain, exacerbating the disease.[12] While these studies provide some evidence of increased inflammatory immune cells infiltrating the CNS following peripheral IL-15 administration, it remains unclear whether CNS inflammation could conversely be reduced by therapeutically depleting IL-15.

Recent work showed that treatment with a rhesusized monoclonal antibody against IL-15 (αIL-15) prior to infection with $SIV_{mac239X}$ resulted in IL-15 depletion *in vivo*, total NK cell ablation, minimal effects on T cell quantities, and subsequently led to increases in plasma viremia and a modest increase in the inflammatory response.[13] However, the impact of this αIL-15 pretreatment on CNS immune and inflammatory responses to acute SIV infection remains unclear. To address this gap, we aimed to investigate several key aspects of the effects of peripheral IL-15 depletion on CNS immune and inflammatory responses to acute SIV infection.

Our study sought to understand how peripheral IL-15 depletion prior to infection influences viral replication and immune responses in the CNS during acute SIV infection (Figure S1). We were further interested in determining whether peripheral modulation of NK cells could alter CNS immune and inflammatory responses to acute SIV infection. Additionally, we aimed to elucidate the specific effects of αIL-15 pretreatment on CNS viral pathogenesis and associated immune and inflammatory responses during this critical early stage of infection.

To address these research objectives, we treated RM with αIL-15 prior to infection with $SIV_{mac}239X$ to determine the effects of IL-15 neutralization on CNS viral pathogenesis and the associated immune and inflammatory response to acute SIV infection. This approach also allowed us to investigate the broader question of whether peripheral modulation of the immune system can influence CNS immune and inflammatory responses.

RESULTS

Histology analysis

Brain tissues from acutely infected RM did not show any significant histological abnormalities at either day 7 or day 14 post-infection. Hematoxylin and eosin staining of tissue sections from different brain regions revealed no remarkable differences between the treatment groups (Figure S2).

Viral load in the brain is independent of plasma viral load

All RMs infected with SIV in this analysis cohort had detectable viral loads in the plasma. αIL-15-treated RM euthanized at 7 days post-infection (dpi) (n = 2) had a mean viral load of 4.57 ± 0.41E10 SIV Gag (Group-Specific Antigen) RNA copies/mL, while αIL-15-treated RM euthanized at 14 dpi had an increased mean viral load of 8 ± 0.25 E10 SIV Gag RNA copies/mL (range = 7.68–8.39E10; Table 1). Quantitative PCR performed to detect SIV in the brain revealed that SIV Gag RNA was below the limit of detection (LOD) at 7 dpi for both αIL-15-treated and untreated animals. However, at 14 dpi, SIV Gag RNA was consistently detected in the frontal cortex (subcortical white matter) of both αIL-15-treated and untreated animals, as well as in the basal ganglia and thalamus, collected from three RMs (Rh11, Rh23, and Rh24), which also showed detectable virus (Table 1). Importantly, there was no significant difference in viral loads between αIL-15-treated and untreated control

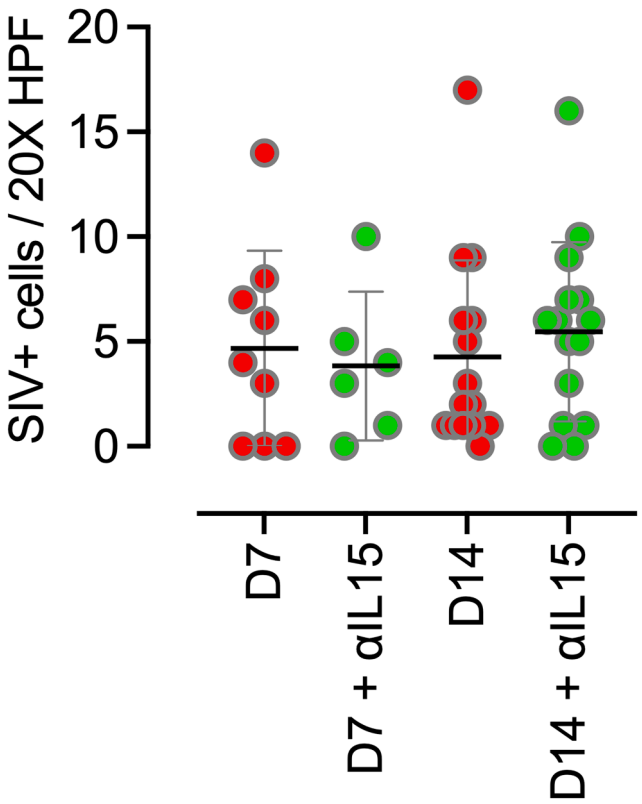

Figure 1. Peripheral IL-15 depletion does not alter the viral load (SIV Gag RNA-positive cells) in the brain

The number of cells positive for SIV RNA in the frontal cortex, thalamus, and basal ganglia was detected using the manual RNAScope 2.5 HD Assay with DAB (3,3'-diaminobenzidine) brown and counted under a light microscope. Each data point represents the average number of SIV-positive cells in one of the brain regions (frontal cortex, thalamus, or basal ganglia), counted at 15 random 20× high-power fields (HPF) per section. Data are presented as mean ± SD. Statistical significance was calculated using a nonparametric Kruskal-Wallis test, and multiple comparisons were assessed using Dunn's post hoc analysis. Day 7 (D7) and day 14 (D14) indicate 7 and 14 days post-infection, respectively; untreated and αIL-15-treated cohorts are shown. All replicates are independent biological replicates.

animals, suggesting that IL-15 depletion did not directly affect viral replication in the brain or plasma at these early time points.

Viral seeding in the brain exhibits compartmentalized clonal expansion

To analyze virus presence in different brain regions, we performed RNA *in situ* hybridization on the frontal cortex, thalamus, and basal ganglia of RM brains (Figure 1). Quantification of SIV-positive cells showed no remarkable differences in SIV quantities between brain regions of αIL-15-treated animals at the two time points (7 and 14 dpi) or in untreated controls at the respective time points. Interestingly, sequence analysis of the viral clones in each brain region showed that the distribution of clonal populations of SIV appears to be compartmentalized in a region-specific manner (Figure S3), with different subsets of viral clones populating distinct regions of the brain. This compartmentalization suggests that viral seeding in the brain may occur through distinct events, leading to the establishment of region-specific viral populations.

αIL-15 treatment alters microglia and astrocyte responses to SIV infection

IL-15 expression in brain tissue was not significantly different between αIL-15-treated groups and untreated groups (Figure 2). While animals with SIV infection had higher levels of IL-15 expression in brain tissue, especially by day 14, the differences did not reach statistical significance. Astrocytes were quantified by GFAP (Glial Fibrillary Acidic Protein) staining in brain tissue and did not show significant changes with αIL-15 treatment or with SIV infection (Figure 2). Microglia were quantified by Iba-1 (Ionized calcium-binding adapter molecule 1) staining and also did not show significant changes with αIL-15 treatment or with SIV infection. SIV-infected groups had higher numbers of astrocytes expressing IL-15 than uninfected groups, although αIL-15-treated groups were not significantly different from untreated groups. Microglial expression of IL-15 was minimal in the brain and did not change with αIL-15 treatment or with infection. However, microglia (stained with Iba-1) revealed changed morphology following αIL-15 treatment (Figure 3). Specifically, we observed that treatment with αIL-15 resulted in increased numbers of ramified microglia in SIV-infected animals, defined as an increased average number of dendritic extensions per cell body in the analyzed areas. While αIL-15 treatment alone did not differ from the untreated group, the αIL-15-treated group with 14 days of SIV infection had more ramified microglia than the untreated group with 14 days of infection. In addition, we also examined neurons in the cortex and did not find significant differences with SIV infection or αIL-15 treatment (Figure S4).

αIL-15 treatment altered T cell quantities in the brain

Peripheral αIL-15 administration significantly abrogated SIV-infection-induced changes in T cell quantities in the brain. In the αIL-15 untreated group of RM, $CD3^+$ T cells (both $CD3^+CD4^+$ and $CD3^+CD4^-$) were lower in quantity at 7 dpi compared with the uninfected and untreated group. T cell numbers were higher at 14 dpi, reaching quantities almost equal to those of uninfected RM. However, in αIL-15-treated RM, there was no such trend observed in $CD3^+$ T cells in general or in the $CD3^+CD4^-$ T cell subset. αIL-15-treated uninfected RM had significantly fewer $CD3^+CD4^-$ T cells in brain tissue compared with untreated and uninfected RM. This difference was not observed between αIL-15-treated and untreated RM infected with SIV at either day 7 or day 14. $CD3^+CD4^+$ T cells exhibited a similar response in the brain parenchymal region, while there were slightly lower numbers of $CD3^+CD4^+$ T cells in the perivascular region at 7 dpi compared with uninfected αIL-15-treated controls; however, this difference was not statistically significant (Figure S5). Interestingly, $CD3^+CD4^+$ T cells in the perivascular space of the untreated group at day 14 of infection appeared to be similar in quantity to those of the untreated and uninfected group.

αIL-15 treatment altered immune cell activation transcriptomics in the brain

Bulk RNA-seq of frontal cortex tissue from RM treated with αIL-15 demonstrated a complex modulation of immune and

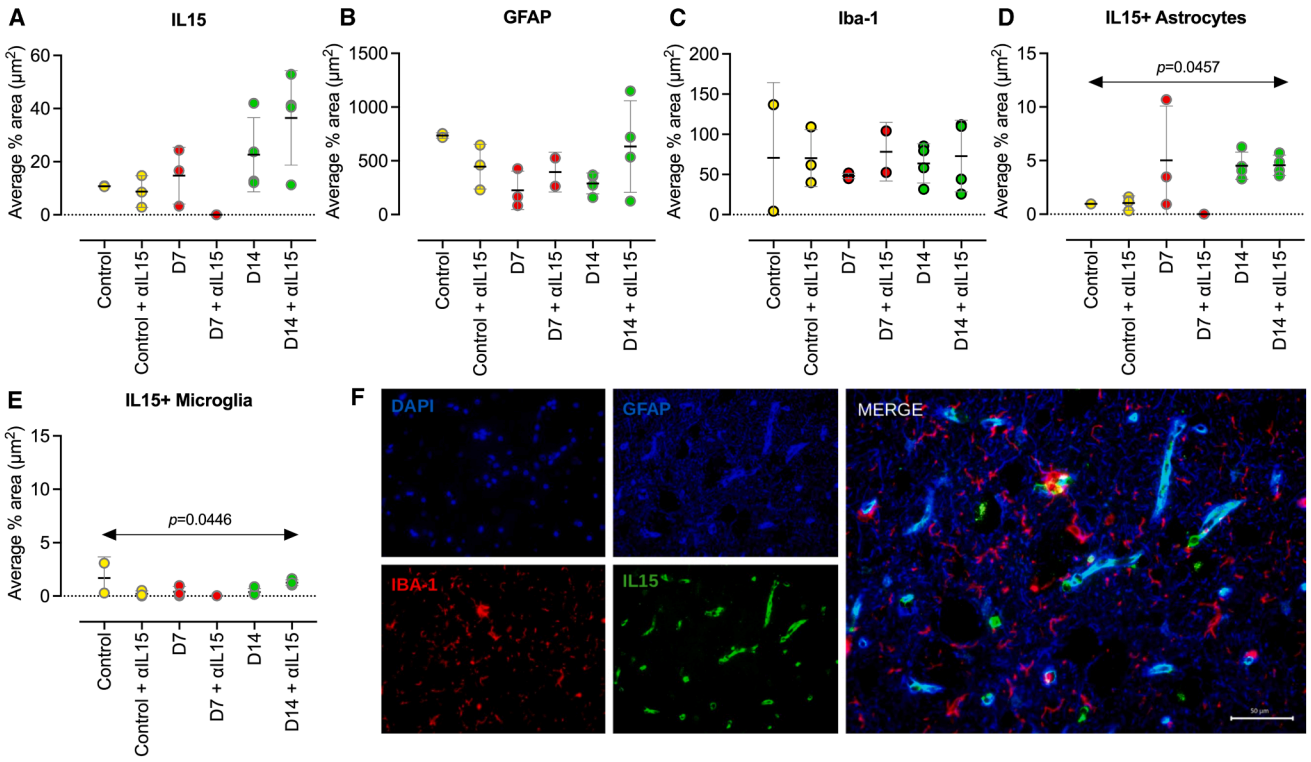

Figure 2. IL-15 expression in the brain tissue

(A) IL-15 expression in the thalamus was not significantly different among the groups.

(B) GFAP expression or (C) Iba-1 expression did not show significant differences between any of the groups.

(D) Colocalization of GFAP and IL-15 showed increased IL-15-expressing astrocytes by day 7 of infection.

(E) Overall decrease of IL-15 expression in microglia.

(F) Representative image of single IHC staining of DAPI (4′,6-diamidino-2-phenylindole) Iba-1, GFAP, and IL-15; the merged image shows co-staining of GFAP, Iba-1, and IL-15. Arrows in (D) and (E) indicate significant differences within the group but not between any specific two groups. Data are presented as mean ± SD. Scale bars, 50 µm. All replicates are independent biological replicates.

inflammatory response gene pathways in response to SIV infection (Figure 4A). Several specific gene pathways were differentially regulated, revealing a nuanced effect of αIL-15 treatment on the CNS immune response. These included IL-6 signaling, as well as the IFN and M1 gene pathways (Figure 4B), which were downregulated following αIL-15 treatment, as were genes associated with oxidative phosphorylation and mitochondrial function (Figure 4C). These RNA transcript changes suggest a shift in the inflammatory profile of the CNS in αIL-15-treated animals.

αIL-15 treatment altered inflammatory cytokine expression in the brain

To further delineate which cells produced the observed inflammatory and anti-inflammatory cytokines, we performed double immunohistochemistry (IHC). While perivascular and parenchymal $CD163^{+}/CD68^{+}$ macrophage quantities were not altered by αIL-15 treatment, their expression of TGF-β was significantly increased in macrophages in the perivascular regions (Figure 5). Proinflammatory cytokine expression in microglia was also modulated by αIL-15 treatment. In contrast, the number of IL-6-expressing microglia in macaques treated with αIL-15 was not significantly different from that of those without treatment. Those infected with SIV after αIL-15 treatment showed significantly fewer microglia expressing IL-6 compared with those infected with SIV without treatment at both day 7 and day 14. (Figure 5). These findings indicate that αIL-15 pretreatment has diverse effects on different cell populations in the CNS, potentially altering the balance between pro- and anti-inflammatory responses to acute SIV infection.

αIL-15 treatment altered inflammatory cytokine expressions in plasma and correlated with myeloid and T cell responses in the frontal cortex and thalamus

We had previously quantified cytokines in the plasma of this cohort of macaques.[13] Correlating these soluble analyte concentrations with the myeloid cell gene transcriptomic signatures from the frontal cortex, we observed that while the myeloid gene pathway signatures correlated positively with the proinflammatory cytokines detected in the plasma of untreated and SIV-infected RM (Figure S6A), those treated with αIL-15 and infected with SIV showed decreased and inverse correlations (Figure S6B). During acute SIV infection, there are increased numbers of perivascular macrophages in the frontal lobe contributing to the myeloid cell gene signature. To examine this further, we quantified IL-18 expression on microglia and

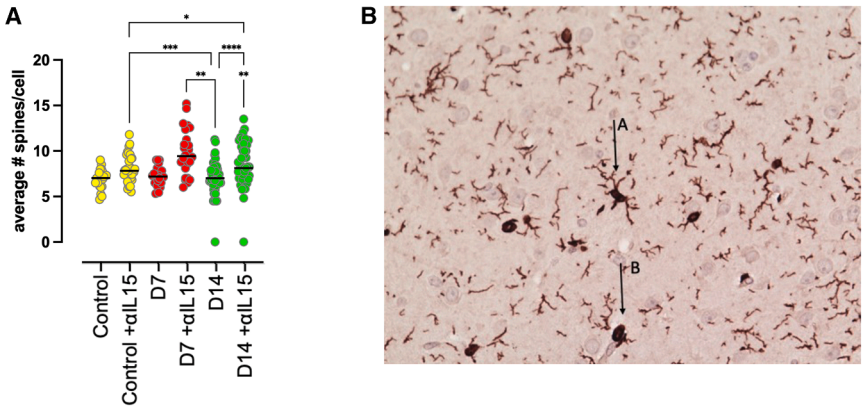

Figure 3. More ramified microglia were detected in rhesus macaques treated with αIL-15 and infected with SIV

(A) Quantification of average spines per cell body in Iba-1-stained RM frontal cortex, imaged at 15 random 40× fields of view (FOV) per section. Each data point indicates the mean value.

(B) Representative image showing Iba-1-positive cell bodies with ramification (arrow A) and cell bodies without ramification (arrow B). Data are presented as mean ± SD. Statistical significance was calculated using a nonparametric Kruskal-Wallis test, and multiple comparisons were assessed using Dunn's post hoc analysis (*$p \leq 0.05$, **$p \leq 0.01$, ***$p \leq 0.001$, and ****$p \leq 0.0001$). Day 7 (D7) and day 14 (D14) indicate 7 and 14 days post-infection, respectively; untreated and αIL-15-treated cohorts are shown. All animals, except the control, were infected with $SIV_{mac}239X$. All replicates are independent biological replicates.

macrophages in the thalamus by IHC (Figure S7). Neither acute SIV infection nor αIL-15 treatment resulted in significantly altered IL-18 expression by microglia or macrophages. Next, we examined G-CSF expression by microglia and macrophages in the thalamus. We found a near-significant ($p = 0.05$) increase in microglial G-CSF expression on day 14 after infection in the αIL-15-treated group (Figure S8).

Correlating brain T cell gene signature pathways with soluble analytes in plasma from day 14 samples, we also observed a significant positive correlation with inflammatory cytokines in frontal cortex samples from the αIL-15-untreated groups with SIV infection (Figure S9A) and decreased and inverse correlations in the αIL-15-treated groups with SIV infection (Figure S9B). We further examined CD137 and Lag 3 expression on $CD3^+$ T cells in the thalamus and did not find any significant differences with SIV infection or α IL-15 treatment (Figure S10). These data indicate that the presence of IL-15 in the periphery is associated with correlative CNS myeloid and T cell migration and proinflammatory responses in acute lentiviral infection.

αIL-15 treatment altered the BBB

We assessed blood-brain barrier (BBB) endothelial integrity by measuring both brain vessel endothelial cell (CD31) expression intensity and by quantifying RM IgG in the brain parenchyma, as previously described.[14] Higher CD31 intensity is indicative of more tightly packed endothelial cells lining the vessels. In contrast, higher quantities of IgG detected in the brain parenchyma indicate loss of BBB integrity, as IgG has leaked across a compromised barrier. While the control group showed a negative correlation between CD31 intensity and IgG quantities, the correlation was no longer significant in the αIL-15-treated group. Additionally, the αIL-15-treated uninfected group showed increased CD31 intensity, whereas intensity was lower in the αIL-15-treated SIV-infected group (Figure S11).

To further assess BBB integrity, we quantified BBB junctional proteins claudin, occludin, and zonula occludens-1 (ZO-1) (Figure 6). αIL-15 treatment did not change the expression of these junctional proteins in uninfected RM. RM treated with αIL-15 treatment had significantly less occludin and ZO-1 expression on day 7 after SIV infection compared with the untreated SIV-infected group. These differences were not present between the treated and the untreated groups at day 14.

Activated RNA gene pathways correlated to mechanisms of brain inflammation

We conducted single-sample gene set enrichment analysis (ssGSEA) to correlate the gene pathways detected in the bulk brain tissue RNA-seq with PCR and histopathological findings. We observed different correlations in the group treated with αIL-15 (Figures S11 and S12). Of significance ($p < 0.05$), in the control group, the gene pathways of NK cells and M2 macrophages were positively correlated with plasma and brain viral loads, quantities of T cells, TGF-β, and IL-2G receptors in the brain. In contrast, in the αIL-15-treated group, the correlations of these two immune cell gene pathways were reduced: NK cell pathways correlated with T cells and TGF-β, whereas the macrophage M2 gene pathway correlated with plasma viral load and TGF-β. The infection-induced activated cytokine pathways, including IL-6, TGF-β, IFN, and TNF-α, correlated positively with plasma viral load (IL-6), IL-2B and IL-2G (TGF-β), macrophages (IFNA), brain viral load, macrophages and T cells (IFNG), and plasma viral load (IFN II and IFN III). The activated cytokine gene pathways in the αIL-15 group also showed different correlations with viral loads and histopathological findings. The IL-6 gene pathways correlated with IHC-quantified IL-6 in brain tissues. The TGF-β gene pathway correlated negatively with IL-2B, IL-2G, and brain viral loads. The antiviral IFN correlated positively with plasma viral loads and TGF-β. Overall, treatment with αIL-15 greatly reduced NK cell gene pathway correlations due to the depletion of these cells, decreased macrophage gene pathway correlations, and altered TGF-β gene pathway correlations, potentially due to the activation of this pathway in a different group of cells.

DISCUSSION

We hypothesized that neuroinflammation during acute SIV infection could stem from the presence of virus in the brain,

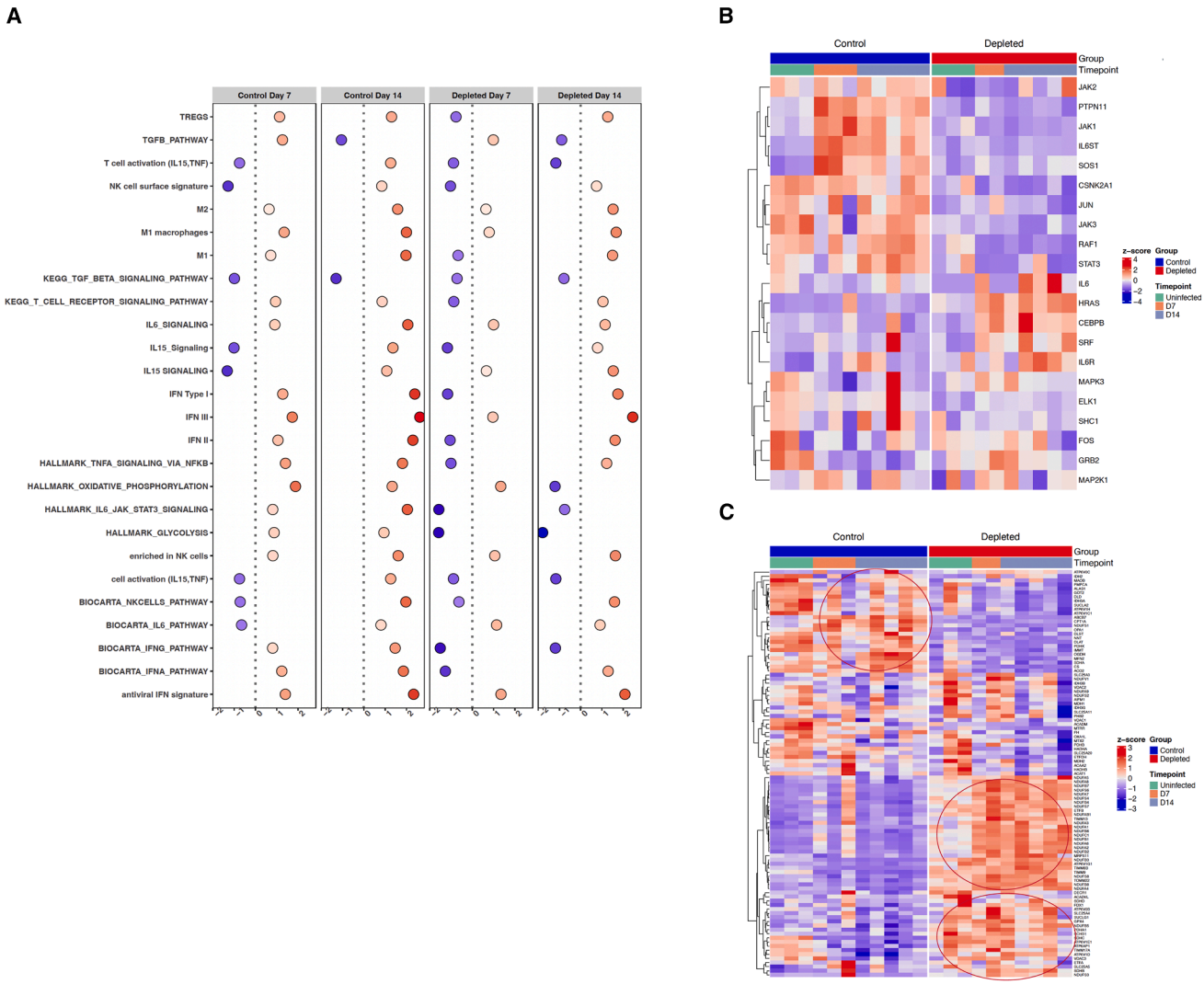

Figure 4. Peripheral IL-15 neutralization modulates inflammatory pathways in the brain

(A) Bubble plots illustrating significantly modulated immune gene pathways in αIL-15-treated and untreated animals. Heatmaps illustrate genes involved in (B) IL-6 signaling and (C) oxidative phosphorylation and mitochondrial regulation. All replicates are independent biological replicates.

proinflammatory cytokines breaching the BBB, or immune cells interacting directly with CNS-resident immune cells or indirectly via cytokine release. This study examined the effect of αIL-15 pretreatment on the CNS response to acute SIV infection at two early time points (7 and 14 dpi). Our findings suggest that the quantities of virus in the CNS may not be the sole driver of neuroinflammation at these early time points, as higher viral loads in brain tissues did not correlate with elevated inflammatory markers compared to tissues with lower viral loads. RM pretreated with peripheral IL-15 exhibited similar CNS SIV viral quantities as those in no-pretreatment infected controls but displayed distinct immune and inflammatory responses. This suggests that αIL-15-mediated immune modulations in the periphery may influence acute inflammatory changes in the brain, as evidenced by analyses of cytokine and gene expression. It should be noted that, while αIL-15 pretreatment did not seem to impact viral quantities in the CNS at these early time points, longer monitoring periods might be necessary to detect such alterations.

Although the role of NK cells in the brain following SIV infection has yet to be fully characterized, they are found to play a significant regulatory role in the murine EAE model and CNS plaques of patients with multiple sclerosis.[15] Prior work in pig-tailed macaques infected with the neurovirulent swarm virus (SIV/17E-Fr and SIV/DeltaB670) linked a strong blood NK cell functional response to improved CNS outcomes.[16] Given the limitations of RM-specific reagents, we are unable to identify NK cells in brain tissues conclusively. However, our research indicates that αIL-15 treatment had implications extending beyond the regulation of viral replication in acute SIV infection. Notably, as αIL-15 treatment could also entail a degree of peripheral $CD8^+$ T cell loss, we cannot fully dismiss the potential

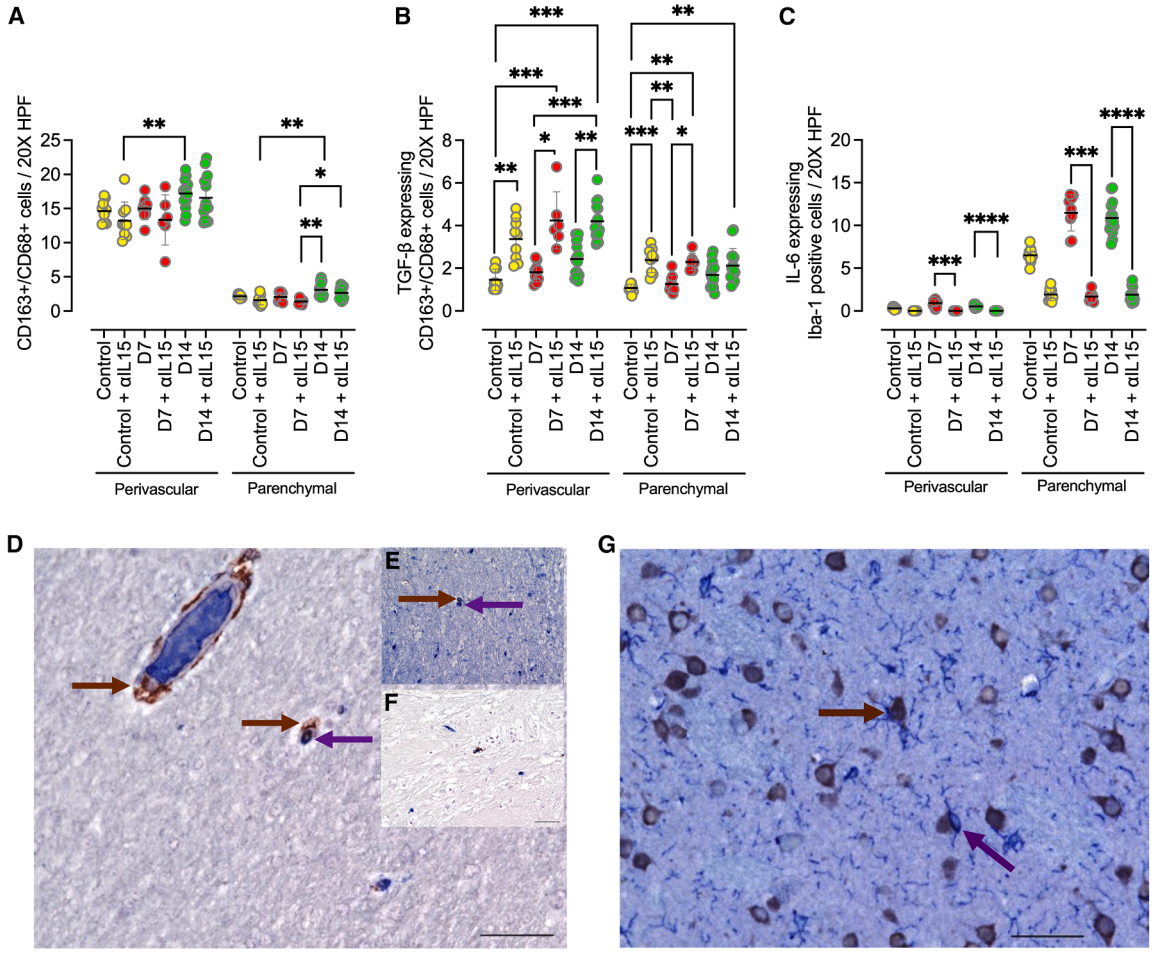

Figure 5. TGF-β-expressing CD163$^+$/CD68$^+$ macrophages increase and IL-6-expressing microglia decrease in different brain regions of rhesus macaques treated with αIL-15 compared to untreated control RM

Each data point represents the average numbers of (A) CD163$^+$/CD68$^+$ macrophages, (B) CD163$^+$/CD68$^+$ macrophages expressing TGF-β, or (C) microglia expressing IL-6 in three brain regions, counted at 15 random 20× high-power fields (HPFs) per section. Representative images for CD163$^+$/CD68$^+$ macrophages (violet arrow) and CD163$^+$/CD68$^+$ macrophages colocalized with TGF-β (brown arrow) are shown in (D and E) basal ganglia and (F) thalamus.

(G) Representative images for Iba-1+ microglia (violet arrow) and Iba-1+ microglia colocalized with IL-6 (brown arrow) at 40×. Data are presented as mean ± SD. Statistical significance was calculated using a nonparametric Kruskal-Wallis test, and multiple comparisons were assessed using Dunn's post hoc analysis (*$p \leq 0.05$, **$p \leq 0.01$, ***$p \leq 0.01$, and ****$p \leq 0.0001$).The scale bar represents 100 μm in (D) and 50 μm in (G). All replicates are independent biological replicates.

involvement of these cells in the observed effects. However, the measured peripheral total T cell quantities did not change with treatment in our cohort.[13]

Our bulk RNA-seq data from frontal cortex tissues showed that peripheral αIL-15 treatment generally decreased the antiviral and anti-inflammatory gene pathways, yet altered macrophage activation toward M1 states. This is further supported by increased gene signatures for IL-6, IL-1β, and TNFα (Figure 4) in the αIL-15 treatment group. It is unclear whether the macrophage changes are due to IL-15 modulation of monocytes in the periphery prior to their migration into the brain tissue or if this is due to a lack of IL-15 stimulation of monocytes/macrophages in either the blood or brain tissue. This drive of monocytes/macrophages toward the M1 state was also associated with increased microglial changes and a surprising reduction in IL-6-positive monocytes/macrophages, as determined by IHC. Though the microglia appeared to exhibit greater ramifications following αIL-15 treatment, these different findings may be due to the single time point examination of the macrophage/monocyte activation process, which represents a continuum between M1 and M2 states.

ssGSEA, in which we correlated the RNA-seq data of activated gene pathways to SIV viral loads in plasma and brain tissues, as well as our histological analysis of brain tissues, further confirmed our findings that treatment with αIL-15 abolished the positive correlations of immune cells (NK cells, T cells, and macrophages) and antiviral activated gene pathways to brain tissue findings. However, the RNA-seq was performed on bulk frontal cortex tissues. Future investigations using spatial transcriptomics and single-cell RNA-seq from multiple brain regions are needed to better define the dynamic immune and inflammatory changes in the brain.

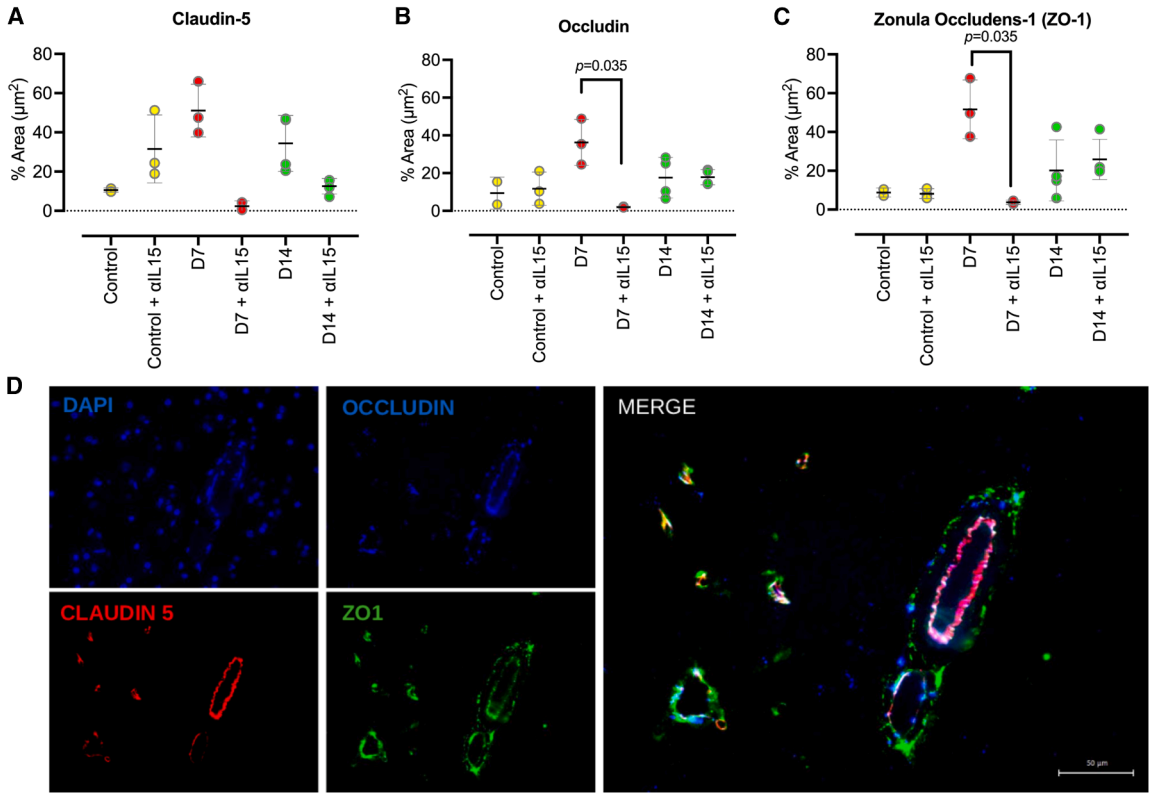

Figure 6. Quantification and imaging of blood-brain barrier junctional proteins

Junctional proteins (A) claudin-5, (B) occludin, and (C) zonula occludens-1 (ZO-1) were analyzed to determine the effects of α-IL-15 treatment. The α-IL-15-treated group on day 7 post-infection showed significantly lower expression of occludin and ZO-1 compared to the untreated group; however, the α-IL-15-treated group on day 14 post-infection did not exhibit any significant differences in expression of these proteins relative to the untreated group.

(D) Representative images of these proteins and their colocalizations. Data are presented as mean ± SD. Scale bars, 50 μm. All replicates are independent biological replicates.

Recently, the FDA approved the use of an IL-15 agonist to stimulate an immune response as part of the treatment for a subtype of bladder cancer.[17] In brain tissue, we did not detect a direct decrease of IL-15 from peripheral treatment with αIL-15. The consequent immune and inflammatory changes in the brain are most likely due to indirect effects of decreased peripheral IL-15. Our data indicate that the consequences of modulating IL-15 pathways in the blood should be examined in end organs, including the brain. For example, RM treated with αIL-15 and infected with SIV had lower quantities of occludin and ZO-1 7 days after infection. While these differences were not detected between groups infected for 14 days, decreases in occludin in CSF have been associated with HAND in PLWH.[18]

The modulation of T cells in various brain tissues and perivascular or parenchymal spaces was also interesting. Although it appears that the general trend was the detection of fewer $CD3^+$ cells per high-power field following αIL-15 treatment, $CD3^+CD4^+$ T cells (as well as $CD3^+CD4^-$ T cells) were at similar levels to control samples from 7 to 14 dpi. Since αIL-15 treatment is expected to remain effective for several weeks to months following administration, this may indicate an expansion of an IL-15-independent T cell population responding to increased viral presence in the brain at 14 dpi. The αIL-15-treated group had fewer $CD3^+CD4^-$ T cells in the brain, even though total peripheral T cell quantities did not decrease.[13] Loss of these cells in the brain may also contribute to the observed decrease in neuroinflammatory response during acute infection but may hinder viral clearance over the long term. Interestingly, αIL-15 treatment resulted in a substantial upregulation of genes associated with oxidative phosphorylation compared to non-depleted animals (Figure 4C). These pathways may alter the inflammatory environment through mTOR signaling,[19] although further studies are required to establish a causal link.

Sequencing analysis of the barcoded virus in this study indicated that, during the acute phase of infection, once a virus seeds a particular region of the brain, it is retained in that location and spreads locally to cells (macrophages, microglia, and others) within the same space but generally does not spread outside the original site within the limited time frame of our study. Our experimental design did not allow us to assess whether specific viral clones could eventually spread to other regions of the brain over time. Longer infection duration studies are needed to determine viral spread within or between the compartmentalized regions of the brain. Nevertheless, because the virus used for infection was barcoded, we were able to

determine the distribution of some viral clones in different brain regions. In regions where we were able to identify the virus, we observed a preference for single clones per region, suggesting that viral seeding is limited and individual lineages can define the predominant population within a small anatomic region. These distinct populations may evolve independently due to local immune pressures or other microenvironmental factors, potentially influencing the course of infection and associated neuropathology in different brain regions. There was no obvious difference in virus seeding between individual sites of the brain in the no-treatment control and the αIL-15-treated samples, although increasing the sample size will be necessary for a more conclusive determination.

Our data showed that peripheral modulation of the immune system prior to acute SIV infection can alter anti-viral immune and inflammatory responses in multiple brain regions. However, the effect of peripheral immune modulation on mitigating HAND, a chronic condition, requires further assessment. Despite this, these findings provide evidence that therapeutics that modulate inflammation in the blood have the potential to decrease inflammation in the brain, thereby aiding in the management of HAND and other neuroinflammatory diseases.

Limitations of the study

While RM infection with SIV closely models human infection and immune response, a limitation of non-human primate studies is the small number of animals in each group. We had originally designed the study for at least three animals in each group. However, one of the day 7 αIL-15-treated animals did not become infected, thus reducing the number in that group to two. This study primarily focused on the frontal cortex because it constitutes the largest part of the brain, providing sufficient tissue material for both RNA-seq and IHC/RNAscope analyses. Analysis of the basal ganglia and thalamus will expand understanding of neuroinflammation. Furthermore, this study did not include neurobehavioral or cognitive assessments, though such changes may not be detectable in RM during acute infection. Lastly, administration of αIL-15 was carried out prior to SIV infection; thus, we are limited in our assessment of the therapeutic use of αIL-15 after infection and how this might influence CNS immune and inflammatory responses.

RESOURCE AVAILABILITY

Lead contact

Requests for further information, resources, and reagents should be directed to the lead contact, C. Sabrina Tan (Sabrina-tan@uiowa.edu).

Materials availability

Regents generated in this study will be made available upon request. Payments and/or a materials transfer agreement may be required.

Data and code availability

- RNA sequencing data have been deposited in GEO (accession number GSE310364) and are publicly accessible at https://www.ncbi.nlm.nih.gov/geo/query/acc.cgi?acc=GSE310364.
- This paper does not report original code.
- Any additional information required to reanalyze the data reported in this paper is available from the lead contact upon request.

ACKNOWLEDGMENTS

Funding acknowledgment: this work was supported by the NIH (K01OD899-03 899-03 and NIA K01899-03 899-03S1 to D.R.R., R33MH112360 to C.S.T., R01AI161010 to R.K.R., and R01NS136448 to M.M.H.).

This project has been funded in part with federal funds from the National Cancer Institute, National Institutes of Health, under contract no. 75N91019D00024. The content of this publication does not necessarily reflect the views or policies of the Department of Health and Human Services, nor does mention of trade names, commercial products, or organizations imply endorsement by the U.S. Government.

We thank Valentin Boero-Teyssie for support with the gene pathway analysis.

AUTHOR CONTRIBUTIONS

C.S.T. and R.K.R. conceptualized the project. C.S.T., R.K.R., D.H.B., B.F.K., and S.E.B. were responsible for the methodology. D.R.R., R.M.G., M.A., K.K., J.M., O.A., E.K.G., C.D., M.M.H., K.L.F., B.T., Y.U., K.L., C.M.F., N.B.M., V.H.-A., R.J., G.W., V.V., and M.L. carried out the investigation. S.E.B., D.H.B., B.F.K., R.K.R., and C.S.T. supervised the project. All authors gave feedback on the manuscript.

DECLARATION OF INTERESTS

The authors declare no conflict of interest.

STAR★METHODS

Detailed methods are provided in the online version of this paper and include the following:

- KEY RESOURCES TABLE
- EXPERIMENTAL MODEL AND STUDY PARTICIPANT DETAILS
- METHOD DETAILS
  - Animals and virus infection
  - Tissue collection and processing
  - Viral load quantification
  - Viral clonal analysis
  - Detection and quantification of SIV RNA-positive cells using RNAscope
  - Single and sequential staining through IHC
  - Microscopy and image analysis
  - Library preparation and bulk RNA-Seq analysis
  - Luminex data analysis
- QUANTIFICATION AND STATISTICAL ANALYSIS

SUPPLEMENTAL INFORMATION

Supplemental information can be found online at https://doi.org/10.1016/j.xcrm.2025.102567.

Received: January 29, 2025
Revised: August 30, 2025
Accepted: December 17, 2025
Published: January 9, 2026

REFERENCES

1. Wei, J., Hou, J., Su, B., Jiang, T., Guo, C., Wang, W., Zhang, Y., Chang, B., Wu, H., and Zhang, T. (2020). The Prevalence of Frascati-Criteria-Based HIV-Associated Neurocognitive Disorder (HAND) in HIV-Infected Adults: A Systematic Review and Meta-Analysis. Front. Neurol. *11*, 581346. https://doi.org/10.3389/fneur.2020.581346.
2. Zenebe, Y., Necho, M., Yimam, W., and Akele, B. (2022). Worldwide Occurrence of HIV-Associated Neurocognitive Disorders and Its

Associated Factors: A Systematic Review and Meta-Analysis. Front. Psychiatry *13*, 814362. https://doi.org/10.3389/fpsyt.2022.814362.

3. Hellmuth, J., Fletcher, J.L.K., Valcour, V., Kroon, E., Ananworanich, J., Intasan, J., Lerdlum, S., Narvid, J., Pothisri, M., Allen, I., et al. (2016). Neurologic signs and symptoms frequently manifest in acute HIV infection. Neurology *87*, 148–154. https://doi.org/10.1212/WNL.0000000000002837.
4. Ulfhammer, G., Edén, A., Antinori, A., Brew, B.J., Calcagno, A., Cinque, P., De Zan, V., Hagberg, L., Lin, A., Nilsson, S., et al. (2022). Cerebrospinal Fluid Viral Load Across the Spectrum of Untreated Human Immunodeficiency Virus Type 1 (HIV-1) Infection: A Cross-Sectional Multicenter Study. Clin. Infect. Dis. *75*, 493–502. https://doi.org/10.1093/cid/ciab943.
5. Gopalakrishnan, R.M., Aid, M., Mercado, N.B., Davis, C., Malik, S., Geiger, E., Varner, V., Jones, R., Bosinger, S.E., Piedra-Mora, C., et al. (2021). Increased IL-6 expression precedes reliable viral detection in the rhesus macaque brain during acute SIV infection. JCI Insight *6*, e152013. https://doi.org/10.1172/jci.insight.152013.
6. Ma, S., Caligiuri, M.A., and Yu, J. (2022). Harnessing IL-15 signaling to potentiate NK cell-mediated cancer immunotherapy. Trends Immunol. *43*, 833–847. https://doi.org/10.1016/j.it.2022.08.004.
7. Harwood, O., and O'Connor, S. (2021). Therapeutic Potential of IL-15 and N-803 in HIV/SIV Infection. Viruses *13*, 1750. https://doi.org/10.3390/v13091750.
8. Younes, S.A., Freeman, M.L., Mudd, J.C., Shive, C.L., Reynaldi, A., Panigrahi, S., Estes, J.D., Deleage, C., Lucero, C., Anderson, J., et al. (2016). IL-15 promotes activation and expansion of CD8+ T cells in HIV-1 infection. J. Clin. Investig. *126*, 2745–2756. https://doi.org/10.1172/JCI85996.
9. Barrenas, F., Hansen, S.G., Law, L., Driscoll, C., Green, R.R., Smith, E., Chang, J., Golez, I., Urion, T., Peng, X., et al. (2021). Interleukin-15 response signature predicts RhCMV/SIV vaccine efficacy. PLoS Pathog. *17*, e1009278. https://doi.org/10.1371/journal.ppat.1009278.
10. Bernard, N.F., Alsulami, K., Pavey, E., and Dupuy, F.P. (2022). NK Cells in Protection from HIV Infection. Viruses *14*, 1143. https://doi.org/10.3390/v14061143.
11. Rentzos, M., Cambouri, C., Rombos, A., Nikolaou, C., Anagnostouli, M., Tsoutsou, A., Dimitrakopoulos, A., Triantafyllou, N., and Vassilopoulos, D. (2006). IL-15 is elevated in serum and cerebrospinal fluid of patients with multiple sclerosis. J. Neurol. Sci. *241*, 25–29. https://doi.org/10.1016/j.jns.2005.10.003.
12. Laurent, C., Deblois, G., Clenet, M.L., Carmena Moratalla, A., Farzam-Kia, N., Girard, M., Duquette, P., Prat, A., Larochelle, C., and Arbour, N. (2021). Interleukin-15 enhances proinflammatory T-cell responses in patients with MS and EAE. Neurol Neuroimmunol Neuroinflamm *8*, e931. https://doi.org/10.1212/NXI.0000000000000931.
13. Woolley, G., Mosher, M., Kroll, K., Jones, R., Hueber, B., Sugawara, S., Manickam, C., Terry, K., Varner, V., Lifton, M., et al. (2023). Natural Killer Cells Regulate Acute SIV Replication, Dissemination, and Inflammation, but Do Not Impact Independent Transmission Events. J. Virol. *97*, e0151922. https://doi.org/10.1128/jvi.01519-22.
14. Byrnes, S.J., Busman-Sahay, K., Angelovich, T.A., Younger, S., Taylor-Brill, S., Nekorchuk, M., Bondoc, S., Dannay, R., Terry, M., Cochrane, C.R., et al. (2023). Chronic immune activation and gut barrier dysfunction is associated with neuroinflammation in ART-suppressed SIV+ rhesus macaques. PLoS Pathog. *19*, e1011290. https://doi.org/10.1371/journal.ppat.1011290.
15. Belien, J., Goris, A., and Matthys, P. (2022). Natural Killer Cells in Multiple Sclerosis: Entering the Stage. Front. Immunol. *13*, 869447. https://doi.org/10.3389/fimmu.2022.869447.
16. Shieh, T.M., Carter, D.L., Blosser, R.L., Mankowski, J.L., Zink, M.C., and Clements, J.E. (2001). Functional analyses of natural killer cells in macaques infected with neurovirulent simian immunodeficiency virus. J. Neurovirol. *7*, 11–24. https://doi.org/10.1080/135502801300069593.
17. Mullard, A. (2024). First-in-class IL-15 receptor agonist nabs FDA approval for bladder cancer. Nat. Rev. Drug Discov. *23*, 410. https://doi.org/10.1038/d41573-024-00073-9.
18. Bai, F., Bono, V., Borghi, L., Bonazza, F., Falcinella, C., Vitaletti, V., Miraglia, F., Trunfio, M., Calcagno, A., Cusato, J., et al. (2024). Association between tight junction proteins and cognitive performance in untreated persons with HIV. AIDS *38*, 1292–1303. https://doi.org/10.1097/QAD.0000000000003923.
19. Mao, Y., van Hoef, V., Zhang, X., Wennerberg, E., Lorent, J., Witt, K., Masvidal, L., Liang, S., Murray, S., Larsson, O., et al. (2016). IL-15 activates mTOR and primes stress-activated gene expression leading to prolonged antitumor capacity of NK cells. Blood *128*, 1475–1489. https://doi.org/10.1182/blood-2016-02-698027.
20. Guide for the Care and Use of Laboratory Animals. The National Academies Collection: Reports funded by National Institutes of Health. 8th ed. Washington DC.
21. Okoye, A.A., DeGottardi, M.Q., Fukazawa, Y., Vaidya, M., Abana, C.O., Konfe, A.L., Fachko, D.N., Duell, D.M., Li, H., Lum, R., et al. (2019). Role of IL-15 Signaling in the Pathogenesis of Simian Immunodeficiency Virus Infection in Rhesus Macaques. J. Immunol. *203*, 2928–2943. https://doi.org/10.4049/jimmunol.1900792.
22. Del Prete, G.Q., Park, H., Fennessey, C.M., Reid, C., Lipkey, L., Newman, L., Oswald, K., Kahl, C., Piatak, M., Jr., Quiñones, O.A., et al. (2014). Molecularly tagged simian immunodeficiency virus SIVmac239 synthetic swarm for tracking independent infection events. J. Virol. *88*, 8077–8090. https://doi.org/10.1128/JVI.01026-14.
23. Whitney, J.B., Hill, A.L., Sanisetty, S., Penaloza-MacMaster, P., Liu, J., Shetty, M., Parenteau, L., Cabral, C., Shields, J., Blackmore, S., et al. (2014). Rapid seeding of the viral reservoir prior to SIV viraemia in rhesus monkeys. Nature *512*, 74–77. https://doi.org/10.1038/nature13594.
24. Cadena, A.M., Ventura, J.D., Abbink, P., Borducchi, E.N., Tuyishime, H., Mercado, N.B., Walker-Sperling, V., Siamatu, M., Liu, P.T., Chandrashekar, A., et al. (2021). Persistence of viral RNA in lymph nodes in ART-suppressed SIV/SHIV-infected Rhesus Macaques. Nat. Commun. *12*, 1474. https://doi.org/10.1038/s41467-021-21724-0.
25. Hensley-McBain, T., Berard, A.R., Manuzak, J.A., Miller, C.J., Zevin, A.S., Polacino, P., Gile, J., Agricola, B., Cameron, M., Hu, S.L., et al. (2018). Intestinal damage precedes mucosal immune dysfunction in SIV infection. Mucosal Immunol. *11*, 1429–1440. https://doi.org/10.1038/s41385-018-0032-5.
26. Wei T, Simko, V. R package 'corrplot': Visualization of a Correlation Matrix (Version 0.92) 2021. Available from: https://github.com/taiyun/corrplot.
27. Gu, Z., Eils, R., and Schlesner, M. (2016). Complex heatmaps reveal patterns and correlations in multidimensional genomic data. Bioinformatics *32*, 2847–2849. https://doi.org/10.1093/bioinformatics/btw313.

STAR★METHODS

KEY RESOURCES TABLE

REAGENT or RESOURCE	SOURCE	IDENTIFIER
Antibodies		
αIL-15 antibody (Lot: SM17-25)	NIH NHP Reagent Resource	N/A
CD3 (clone F7.2.38), 1:200	Agilent-Dako	AB_2631163
CD4 (clone 4B12), 1:200	Agilent-Dako	AB_2728838
GFAP (pAb number: Z0334), 1:500	Agilent-Dako	AB_10013382
CD163 (clone EDHu1), 1:1000	BioRad	AB_2074540
CD68 (clone 298807), 1:500	R&D Systems	AB_2074834
Iba-1 (pAb Catalog: 019–19741), 1:1000	FUJIFILM Wako	AB_839504
IL-6 (ab219758), 1:1000	Abcam	N/A
TGF-β (EPR21143), 1:1000	Abcam	AB_2893156
Claudin-5 (EPR7583), 1:500	Abcam	AB_11157940
Occludin (OC-3F10), 1:100	ThermoFisher Scientific/Invitrogen	AB_2533101
Zonula occludens −1 (ZO1-1A12), 1:200	ThermoFisher Scientific/Invitrogen	AB_3074173
IL-15 (E−4), 1:250	Santa Cruz	AB_2124575
IL-18 (PA5110679), 1:250	ThermoFisher Scientific/Invitrogen	AB_2856090
G-CSF (BVD13-3A5), 1:500	ThermoFisher Scientific/Invitrogen	AB_2536268
Lag 3 (EPR20261), 1:100	Abcam	AB_2883982
CD137 (EPR25096-57), 1:500	Abcam	N/A
NeuN (ab104225), 1:500	Abcam	AB_10711153
CXCL12 (EPR1216), 1:200	Abcam	AB_2894874
Bacterial and virus strains		
$SIV_{mac239X}$	NIH	N/A
Chemicals, peptides, and recombinant proteins		
RNAlater	ThermoFisher	AM7020
RNase		N/A
Critical commercial assays		
Qiagen Viral RNA kit	Qiagen	52904
TaqMan Fast Advanced Master Mix	ThermoFisher	4444965
RNeasy 96 QIAcube HT kit	Qiagen	74171
QIAamp 96 QIAcube HT kit	Qiagen	57731
Superscript III VILO	Invitrogen	11754050
AmpliCapMax T7 High Yield Message Maker kit	Qiagen	52904
RNA Clean and Concentrator kit	ThermoFisher	4444965
RNAscope™ Multiplex Fluorescent V2	Qiagen	74171
RNAscope™ 2.5 HD Assay-Brown Kits	Qiagen	57731
Deposited data		
RNAseq rhesus macaques frontal cortex subcortical white matter	NIH	GSE310364
Experimental models: Organisms/strains		
Indian Rhesus Macaques	Biomere (MA)	N/A
Oligonucleotides		
sGag21 (forward) GTCTGCGTCATCTGGTGCATTC	IDT	N/A
sGag22 (reverse) CACTAGGTGTCTCTGCACTATCTGTTTTG	IDT	N/A

(*Continued on next page*)

Continued

REAGENT or RESOURCE	SOURCE	IDENTIFIER
sGag23 (probe) 5′FAM-CTTCCTCAGTGTG TTTCACTTTCTCTTCTGCG-BHQ-3′	IDT	N/A
SIV *gag* probes **RNAscope™ Probe - V-SIVmac251-gag**	ACD	Cat # 488091
Software and algorithms		
Hybrid Cell counting	Keyence	BZH4-C & BZH4-CM
QuantStudio Software v1.3	ThermoFisher	N/A
R v4.4.2	r-project.org	N/A
GraphPad Prism 9.0	GraphPad Software	N/A

EXPERIMENTAL MODEL AND STUDY PARTICIPANT DETAILS

This study was based on analysis of $SIV_{mac239x}$ infected adult male RM (*Macaca mulatta*) of Indian origin, ages 4–10 years. The animals were housed and cared for at Biomere Inc. (Worcester, MA) under the rules and regulations of the Committee on the Care and Use of Laboratory Animal Resources and, in agreement with the American Association for Accreditation of Laboratory Animal Care standards and Guide for the Care and Use of Laboratory Animals.[20] Animals were fed a standard diet.

METHOD DETAILS

Animals and virus infection

Animal care and viral infection procedures were conducted as previously described by our group.[13] Peripheral administration of αIL-15 antibody (Lot: SM17-25; kindly provided by the NIH NHP Reagent Resource) was given intravenously at day −21 (20mg/kg) and day −7 (10mg/kg) relative to $SIV_{mac239X}$ inoculation prior to infection, based on prior study protocols.[13,21] The animals were infected intrarectally with a single dose of 300,000–500,000 IU of SIV_{mac}239X (Table S1). This virus stock contained nine isogenic and sequence-discriminable molecularly tagged variants (variants A to I) plus wild-type (WT) SIV_{mac}239X (10 in total) within a single inoculum stock, with equal proportions of all genotypes.[22] RM were necropsied either at 7 or 14 days post-infection (dpi) (Figure S1). The right-sided heart was perfused with cold PBS during necropsy to decrease blood cell contamination in the brain tissues.

Tissue collection and processing

Brains were harvested, and tissue samples (roughly 1 cm × 1 cm × 1 cm) were collected from the frontal cortex of one of the hemispheres and cryopreserved in RNAlater for assessing viral load and for RNA-Seq analysis. The other hemisphere was stored in 10% neutral buffered formalin for 14 days, after which the hemisphere was sliced and tissue samples were collected from different brain regions (frontal cortex, thalamus, basal ganglia), embedded in paraffin, and sectioned at 10 μm thickness for *in situ* hybridization (ISH) and immunohistochemistry (IHC) studies. The sectioned tissues on glass slides were stored under vacuum conditions until used. A tissue section from each brain region was also stained with H&E for routine histological analysis.

Viral load quantification

Peripheral viral loads were quantified as previously described.[23] In brief, the known amount of RNA extracted from cell-free plasma was reverse-transcribed to cDNA using *gag*-specific primers, followed by RNase treatment at 37°C for 20 min. Then, cDNA amplification was performed using a 7300 ABI Real-Time PCR system (Applied Biosystems) according to the manufacturer's protocol (TaqMan Fast Advanced Master Mix User Guide; publication 4444605). All reactions were run in triplicate, and a SIV-*gag* RNA standard was included.

Brain viral load was determined by quantifying both DNA and RNA through qPCR as described earlier.[24] In short, total RNA (using the RNeasy 96 QIAcube HT kit) and genomic DNA (using the QIAamp 96 QIAcube HT kit) were isolated from frozen brains according to the manufacturer's protocol (Qiagen). Following RNA extraction, the total RNA was converted to cDNA using Superscript III VILO (Invitrogen) using the manufacturer's specifications. Viral Gag copies were determined using the QuantStudio 6 Flex system (Applied Biosystems) following previously optimized thermocycler settings, with the following protocol repeated for 45 cycles: 95°C for 20 s for initial denaturation, followed by 95°C for 1 s and 60°C for 20 s. SIV Gag-specific primers and probes that were used for the assays are as follows: sGag21 (forward) GTCTGCGTCATCTGGTGCATTC, sGag22 (reverse) CACTAGGTGTCTCTGCACTATCTGTTTTG, and sGag23 (probe) 5′FAM-CTTCCTCAGTGTGTTTCACTTTCTCTTCTGCG-BHQ-3′. RT-PCR assays were run in duplicate, whereas the viral DNA assays were run in triplicate. To calculate SIV Gag DNA and RNA copies, standards were used. For preparing RNA standards, the AmpliCapMax T7 High Yield Message Maker kit (Cell Script) was used, followed by RNA purification using an RNA Clean and Concentrator kit (Zymo Research). RNA standards were prepared in log dilutions, and standards were used in each RT-PCR assay. For the SIV DNA PCR assay, an RPP30 control was also included. Viral RNA load was calculated as RNA copies

per microgram of total input RNA. LOD for the SIV RNA assay was one copy per μg of total RNA input. Viral DNA load was calculated as SIV Gag DNA copies per million cells, after normalizing DNA copies to the total number of input cells. Each cell has two copies of the RPP30 gene. LOD for the SIV DNA assay was eight copies per million cells.

Viral clonal analysis

Viral RNA was extracted from the tissues using a Qiagen Viral RNA kit. Next-generation sequencing analysis was performed as previously described.[13,25]

Detection and quantification of SIV RNA-positive cells using RNAscope

Cells positive for SIV RNA (in basal ganglia, thalamus, and frontal cortex) were detected and quantified using RNAscope Multiplex Fluorescent V2 and RNAscope 2.5 HD Assay-Brown Kits (Advanced Cell Diagnostics, Inc.), respectively. SIV *gag* probes against the *gag* region of SIV purchased from Advanced Cell Diagnostics, Inc., were used for quantifying SIV RNA-positive cells by RNAscope 2.5 HD Assay-Brown Kit following the manufacturer's instructions.

Single and sequential staining through IHC

Manual IHC with different chromogenic substrates was used for single-antigen detection or for detecting two antigens simultaneously using a sequential double-staining approach. Immune cell markers, including CD3 (clone F7.2.38), CD4 (clone 4B12), and GFAP (pAb number: Z0334) from Agilent-Dako; CD163 (clone EDHu1) from BioRad; CD68 (clone 298807) from R&D Systems; Iba-1 (pAb Catalog: 019–19741) from FUJIFILM Wako, were used for single antigen detection. Cells positive for proinflammatory IL-6 (ab219758) and anti-inflammatory TGF-β (EPR21143), both from Abcam, Claudin-5 (EPR7583), occludin (OC-3F10), zonula occludens −1 (ZO1-1A12), IL-15 (E−4), IL-18 (PIPA5110679), G-CSF (BVD13-3A5), Lag 3 (EPR20261), CD137 (EPR25096-57), NeuN (ab104225), CXCL12 (EPR1216), were identified by staining for either of the cytokines followed by staining for one of the immune cell markers mentioned above. Standard IHC protocol was followed.

Tissue sections stained for Iba-1 were also used to assess the change in microglia morphology. Morphology analysis was carried out by counting the number of spines attached to the cell body per 40x high-power frame and averaging the number of spines by the number of microglial cell bodies per frame. For each slide, an average of 15 randomly selected frames was analyzed. The spine counting was performed manually by different individuals who were blinded to the sample name/group to minimize person-to-person bias in the counting, and the distribution of data was found to be unbiased.

Microscopy and image analysis

RNAscope detection and imaging were performed using a Zeiss LSM 880 laser scanning confocal microscope, with at least 20 high-power fields (HPFs) per slide imaged at 20X magnification. Slides from single and double IHC were imaged in a Zeiss Axio Imager M1 microscope. At least 20 HPFs at 20X or 40X were captured for each section. For each section, 15 HPF images were randomly chosen for quantification. While counting the total number of positively stained cells in single or double IHC, the positively stained cells were also sub-classified based on their location: as perivascular (V) if they lined the blood vessel, or parenchymal (P) if they were present in the brain parenchyma. Cell counts are expressed as an average calculated across the number of images quantified (15 fields of view). Expression of GFAP and Iba-1 was quantified using the Keyence microscope analysis program by quantifying the intensity of staining, performing pixel analysis of colocalizations, and normalizing to DAPI staining in each field of view.

Library preparation and bulk RNA-Seq analysis

RNA was isolated from bulk brain frontal cortex tissues, processed, and analyzed as previously described.[5] Single-sample Gene Set Enrichment Analysis (ssGSEA) was performed following the protocol described by Pranali (2021), https://rpubs.com/pranali018/SSGSEA. ssGSEA scores, which represent up- or down-regulated gene pathway scores per sample, were correlated with clinical measures using the corrplot package[26] and visualized using both corrplot and ComplexHeatmap.[27]

Luminex data analysis

Luminex data were obtained from a previously published manuscript utilizing this animal cohort.[13] Luminex values were loaded into R v4.4.2. Single-sample Gene Set Enrichment Analysis (ssGSEA) scores were calculated for each bulk RNA-seq sample. Correlations between Luminex analyte values and ssGSEA scores were calculated using the cor() function from the base stats package. P-values were obtained with the cor.mtest() function from the corrplot[26] package. Correlations of interest were visualized with the corrplot functions.

QUANTIFICATION AND STATISTICAL ANALYSIS

Unless otherwise mentioned, GraphPad Prism 9.0 was used for all statistical analyses. A nonparametric Kruskal-Wallis test was used for analysis, and multiple comparisons were assessed using Dunn's post hoc analysis. Unless otherwise stated, data are presented as mean ± standard deviation (SD). *p* values (multiplicity-adjusted *p* values for multiple comparisons) were considered significant when $*p < 0.05$, $**p < 0.01$, $***p < 0.001$, and $****p < 0.0001$, while ns indicates $p > 0.05$, which means no significance.